5692–5703 *Nucleic Acids Research, 2011, Vol. 39, No. 13* *Published online 29 March 2011*
doi:10.1093/nar/gkr148

Analysis of microRNA turnover in mammalian cells following *Dicer1* ablation

Michael P. Gantier[1], Claire E. McCoy[1], Irina Rusinova[2], Damien Saulep[3], Die Wang[1], Dakang Xu[1], Aaron T. Irving[1], Mark A. Behlke[4], Paul J. Hertzog[2], Fabienne Mackay[3] and Bryan R. G. Williams[1,*]

[1]Centre for Cancer Research, [2]Centre for Innate Immunity and Infectious Diseases, Monash Institute of Medical Research, Monash University, Clayton, Victoria 3168, [3]Department of Immunology, Monash University, Alfred Medical Research and Education Precinct, Melbourne, Victoria 3004, Australia and [4]Integrated DNA Technologies Inc., Coralville, IA 52241, USA

Received January 10, 2011; Revised February 27, 2011; Accepted February 28, 2011

ABSTRACT

Although microRNAs (miRNAs) are key regulators of gene expression, little is known of their overall persistence in the cell following processing. Characterization of such persistence is key to the full appreciation of their regulatory roles. Accordingly, we measured miRNA decay rates in mouse embryonic fibroblasts following loss of Dicer1 enzymatic activity. The results confirm the inherent stability of miRNAs, the intracellular levels of which were mostly affected by cell division. Using the decay rates of a panel of six miRNAs representative of the global trend of miRNA decay, we establish a mathematical model of miRNA turnover and determine an average miRNA half-life of 119 h (i.e. ~5 days). In addition, we demonstrate that select miRNAs turnover more rapidly than others. This study constitutes, to our knowledge, the first in-depth characterization of miRNA decay in mammalian cells. Our findings indicate that miRNAs are up to 10× more stable than messenger RNA and support the existence of novel mechanism(s) controlling selective miRNA cellular concentration and function.

INTRODUCTION

It is now well-established that microRNAs (miRNAs) are master regulators of most cellular processes. Many viruses utilize viral-encoded miRNAs during their infectious cycle (1), mice lacking miRNAs are not viable (2,3) and miRNA levels are altered in most cancers (4). miRNAs are short single-stranded RNAs of ~22 nt processed from longer RNA primary transcripts (pri-miRNAs) with high secondary structure. Canonical processing of pri-miRNA into mature miRNA requires sequential cleavage of the pri-miRNA into a ~70-nt miRNA precursor by the endonuclease Drosha (5), and subsequent cleavage into a ~20-bp miRNA duplex by the endonuclease Dicer1 (6). One strand of this duplex is loaded onto the RNA-induced silencing complex (RISC) forming the miRISC regulating cognate messenger RNA (mRNA) stability in GW bodies (7).

The canonical biogenesis of miRNAs is regulated by several mechanisms that directly impact on the overall production of mature miRNAs (8). For instance, LIN-28 affects the processing of let-7 precursors by Drosha and Dicer1, allowing it to specifically switch-off the production of mature forms of let-7 in undifferentiated embryonic stem cells (8,9). Such regulation of miRNA processing fine-tunes their intracellular levels, and modulates their biological activity. Indeed, miRNA intracellular concentration directly relates to their ability to affect mRNA translation with a suggested threshold of about 100 molecules per cell required for function (10). Because the intracellular miRNA steady-state levels result from not only the synthesis of new miRNAs but also the degradation of previously synthesized miRNAs, characterization of miRNA persistence following processing is crucial to the understanding of their biological function.

However, what happens to mature miRNAs is currently poorly understood, and their overall persistence following Dicer1 processing is inferred to be 'highly stable' from studies of select miRNAs (8,11). For instance, miR-208 was found to persist in the absence of its precursor for

*To whom correspondence should be addressed. Tel: +613 9594 7166; Fax: +613 9594 7167; Email: bryan.williams@monash.edu

The authors wish it to be known that, in their opinion, the first two authors should be regarded as joint First Authors.

>12 days in heart tissue (12) and miR-122 levels remained unchanged following rapid decrease of pri-miR-122 in liver tissue (13). Conversely, a rapid decrease of miRNAs has been observed in neuronal cells, following blocking of pri-miRNA transcription (14). Furthermore, selective miRNA stability has been proposed to be impacted on by various factors, including 3′ base modifications (15), the degree of complementarity to the target (16) or target abundance (17). With the exception of miR-451 (18), miRNAs are dependent on Dicer1 maturation to be able to exert their regulatory function (19,20). Consequently, different approaches have been developed to disrupt Dicer1 function and characterize the regulatory roles of miRNAs. To our knowledge, the use of an inducible deletion of *Dicer1* to address miRNAs decay has not been previously adopted.

Here, we investigate the stability of miRNAs following a global shutdown of miRNA synthesis. Relying on the inducible genetic ablation of *Dicer1* in immortalized embryonic fibroblast cells, we modelled miRNA decay in a theoretical non-dividing cell and established that the average miRNA half-life is about 10× that of mRNA, i.e. about 5 days. In addition, we observed significant variations in select miRNA half-lives, thereby supporting the existence of novel mechanism(s) regulating miRNA function through fine-tuning of steady-state miRNA levels.

METHODS

Ethics statement

The use of animals and experimental procedures were approved by Monash Medical Centre Ethics Committee under references MMCA/2008/26/BC and MMCA 2007/07.

Cell culture

Dicer1$^{flox/flox}$ mice (a kind gift from M. McManus, University of California, San Francisco, CA, USA) (21) were bred to *R26CreER* mice expressing the Cre/Esr1 fusion protein from the *ROSA26* locus (22). Mouse embryonic fibroblasts (MEFs) from Day 14 embryos were immortalized following transfection of pSG5-SV40-LT-Ag (a kind gift from D. Huang, Walter and Eliza Hall Institute of Medical Research, Melbourne, Australia) and six successive 1/10 passages. For stable enhanced green fluorescent protein (EGFP) expression, the MEFs were transduced with an EGPF-expressing lentiviral construct (pLV-CMV-GFP). Bone marrow was isolated from the femurs of *Dicer1*$^{flox/flox}$ *xCre/Esr1* mice, and primary bone marrow derived macrophages (BMDMs) were differentiated in 20% L929-cell-conditioned medium for 7 days at 37°C in a 5% CO_2 atmosphere. BMDMs, MEFs and HEK293T cells stably expressing GFP (23) were cultured in complete Dulbecco's modified Eagle's medium (DMEM) (cat. no. 11965-092; Invitrogen Corporation, Carlsbad, CA, USA) supplemented with 10% sterile foetal bovine serum (#FBS-500, ICPBio Ltd, Auckland, New Zealand) and 1× antibiotic/anti-mycotic (Invitrogen) (referred to as complete DMEM). Splenic B cells were purified using a B Cell Isolation Kit (depletion of non-B cells) from Miltenyi Biotech. Purity was >95%. Activation of splenic B lymphocytes was performed in Roswell Park Memorial Institute (RPMI) 1640 + L-glutamine medium (#11875085, Invitrogen) supplemented with 10% FBS, 55 mM β–mercaptoethanol, 2 mM L-glutamine, 10 mM HEPES and 100 U/ml of penicillin–streptomycin, and cells were stimulated with LPS (25 μg/ml, InvivoGen, San Diego, CA, USA) and murine interleukin 4 (10 ng/ml, eBioscience, San Diego, CA, USA) for the indicated amount of time.

OHT treatment of the cells

Hydroxy-tamoxifen (OHT) (H7904-5 mg, Sigma Aldrich, St Louis, MO, USA) was resuspended in 0.5 ml of 100% ethanol (resulting in stock solution at ∼25 mM) kept at −80°C. Prior to cell treatment, the stock solution was first diluted to 2.5 mM in 100% ethanol before being diluted further to the final concentration in complete DMEM. For OHT treatment of BMDMs, the cells were differentiated in 20% L929-cell-conditioned medium, and were washed on Day 3 with fresh medium supplemented with 20% L929-cell-conditioned medium and 500 nM OHT. The cells were collected on Day 5 and plated in 24-well plates in 20% L929-cell-conditioned medium, and collected at Days 6–9 for RNA extraction.

Reverse transcription quantitative real-time PCR

Total RNA containing small RNAs was purified from cultured cells using an adapted RNeasy protocol (Qiagen, Valencia, CA, USA) or the mirVana miRNA isolation kit (Ambion, Austin, TX, USA). For mRNA quantification, cDNA was synthesized from isolated RNA using the High-capacity cDNA archive kit (Applied Biosystems, Foster City, CA, USA) according to the manufacturer's instructions. Reverse transcription quantitative real-time polymerase chain reaction (RT-qPCR) was carried out with the SYBR GreenER™ qPCR SuperMix for iCycler® instrument (#11761-500; Invitrogen Corporation). Murine glyceraldehyde 3-phosphate dehydrogenase (mGAPDH) (NM_008084) was used as reference gene and amplified with the following primer pair: mGAPDH-FWD: TTCACCACCATGGAGAAGGC; mGAPDH-REV: GGCATGGACTGTGGTCATGA. Detection of the primary miRNAs was carried out with the following primer pairs: Mir155 (NR_029565.1)—pri-miR-155-FWD: AAACCAGGAAGGGGAAGTGT (24); pri-miR-155-REV: ATCCAGCAGGGTGACTCTTG (24); Mir146a (NR_029558.1)—pri-miR-146 a-FWD: GTGTGTATCCCCAGCTCTGA; pri-miR-146 a-REV: CTTCACCCCACTCTCTCCAC; Mir21 (NR_029738.1)—pri-miR-21-FWD: TGTACCACCTTGTCGGATAGC; pri-miR-21-REV: AAGGGCTCCAAGTCTCACAA. Wild-type Dicer1 mRNA (NM_148948.2) was detected with mDicer1-RT-FWD: TCTGCAGGCTTTTACACACG and mDicer1-Exon-REV: CCAATGATGCAAAGATGGTG. Each amplicon was sequence verified and used to generate a standard curve for the quantification of gene expression. For mature miRNA detection, miRNA TaqMan® assays (Applied Biosystems) for the indicated miRNAs were used according to the manufacturer's instructions, where

10–30 ng of total RNA was reverse transcribed with pools of up to eight miRNA-specific reverse transcription primers (with the TaqMan® MicroRNA Reverse Transcription Kit). With the exception of mmu-miR-155 and snoRNA202, all the individual Taqman® assays used were compatible between human and mouse. miRNA levels were determined by RT-qPCR with the TaqMan® Universal PCR Master Mix on a 7900 RT-PCR system (Applied Biosystems), and fold changes in expression were calculated by the $2^{-\Delta\Delta Cq}$ (C_q = quantification cycle) method using snoRNA202 (for all mouse experiments), or miR-16 (for HEK293T cells) as reference genes.

Low density miRNA arrays

TaqMan® Array Rodent MicroRNA (A Cards v2.0, Applied Biosystems) were used for the global detection of miRNAs from one biological sample set. Briefly, 900 ng of total RNA containing small RNAs was reverse transcribed using the Megaplex™ RT Primers, Rodent Pool A (Applied Biosystems) with the TaqMan® MicroRNA Reverse Transcription Kit and each plate was consecutively ran using the TaqMan® Universal Master Mix II on the 7900 RT-PCR system, according to the manufacturer's instructions. Simultaneous analysis of the three different plates (one plate at Days 3–5) was carried out using the RQ Manager software. To determine significant miRNA expression, we performed the following filtering. (i) We only considered miRNAs that had C_q values lower than 37 for all three time-points. (ii) We used the average of four RNAU6 probes present on each array as reference gene (giving ΔC_q values), and calculated $\Delta\Delta C_q$ values using Day 3 as control condition. Fold decrease of miRNA levels relative to Day 3 was inferred using $2^{(-\Delta\Delta Cq)}$ values. (iii) We limited our analysis to miRNAs levels that consistently decreased with time (i.e. Day 3 > Day 4 > Day 5)—hereby identifying 104 miRNAs. Importantly, out of the 158 miRNAs detected by PCR-array with C_{qs} inferior to 37 at each time-point, 17 were such that the concentrations of miRNAs at Day 3 > Day 4 and Day 3 > Day 5 but not Day 4 > Day 5, 21 had increased miRNA expression at either Day 4 or Day 5 compared with Day 3 (most likely from technical PCR outlier) and 17 did not decrease with time (i.e. Day 3 ≤ Day 4 ≤ Day 5) (Supplementary Table S1). Recent evidence suggests that five of these non-decreasing RNAs (miR-509-3 p, miR-658, miR-207, miR-680 and miR-687—see Supplementary Table S1 in bold) would in fact not be miRNAs (25), hence validating our method of discrimination and the robustness of the RT-qPCR array platform. Our data on 104 miRNAs, therefore, rely on 3/4 of the miRNA possibly expressed by the MEFs, and a less conservative approach including the 17 miRNAs with decreased expression at Days 4 and 5 compared with Day 3 gave very similar averaged decrease (data not shown). Similar results were obtained using normalization to other controls such as snoRNA202 or snoRNA135.

To account for possibly rapidly decaying miRNAs that would not be detected after Day 3, we also analysed the global trend of miRNA decay between Days 3 and 4 (Supplementary Table S2), and Days 4 and 5 (Supplementary Table S3), including miRNAs that were not detected at one of the time-points (C_q = 40). (i) We only considered miRNAs that had Cq values lower than 40 at Day 3, and (ii) that had a lower C_q value at Day 3 than Day 4. One hundred and eighty-three miRNAs matched these criteria, with an averaged 64% decrease of miRNA expression between Days 3 and 4 (when normalized to RNAU6 as detailed above). (iii) We next repeated this analysis and assessed the expression of miRNAs between Days 4 and 5, filtering miRNAs that had C_q values lower than 40 at Day 4, and a lower C_q value at Day 4 than Day 5. One hundred and fifty-four miRNAs matched these criteria, with an averaged 68% decrease of miRNA expression between Days 4 and 5. These data, although approximate given that the non-detected miRNAs were attributed an arbitrary C_q value of 40, support our claim that the global trend of miRNA decay is constant between Days 3 and 4, and 4 and 5, even when including miRNAs that are possibly rapidly degraded.

Synthetic RNAs

All small interfering RNA (siRNA) and si-miRNA duplexes were synthesized as single-stranded RNAs by Integrated DNA Technologies (IDT) with HPLC purification, and resuspended in duplex buffer (100 mM potassium acetate, 30 mM HEPES, pH 7.5, DNase–RNase free H_2O) to a concentration of 80 μM. Annealing was performed by incubating the complementary single-stranded RNAs at 92°C for 2 min and leaving them for 30 min at room temperature (giving a final concentration of 40 μM). miR-155-S: 5′ CCCUAUCACAAUUAGCAUUAAUU; miR-155-AS: 5′ UUAAUGCUAAUUGUGAUAGGGG U. miR-21-S: 5′ AACAUCAGUCUGAUAAGCUAUU; miR-21-AS: 5′ UAGCUUAUCAGACUGAUGUUGA.

Reverse transfection of small RNAs

For Figure 1D, 4.5 μl of Lipofectamine 2000 was diluted in 300 μl of Opti-MEM and 2.25 μl of mi-siRNA molecules (diluted to 4 μM in duplex buffer) was added such that the final concentration of each siRNA was 5 nM per well (the volumes indicated are for biological triplicate). After 20 min of incubation, 100 μl of the mix was added directly into each well of a 24-well plate. HEK293T-GFP cells (100 000) resuspended in 500 μl of antibiotic-free DMEM (supplemented with 10% FBS) were added to each well giving a final volume of 600 μl/well. The cells were incubated at 37°C for 7 h before being washed with fresh medium. For Figure 2B, 4.8 μl of Lipofectamine 2000 was diluted in 300 μl of Opti-MEM and 3 μl of siRNA molecules (diluted to 4 μM in duplex buffer) was added such that the final concentration of siRNA in each well was 10 nM (the volumes indicated are for biological triplicate in two cell types). After 20 min of incubation, 50 μl of the mix was added directly into each well of a 96-well plate (in triplicate for each cell type). MEFs (20 000; previously treated with OHT or not) in 150 μl of antibiotic-free DMEM (supplemented with 10% FBS) were added to each well giving a final volume of 200 μl/well.

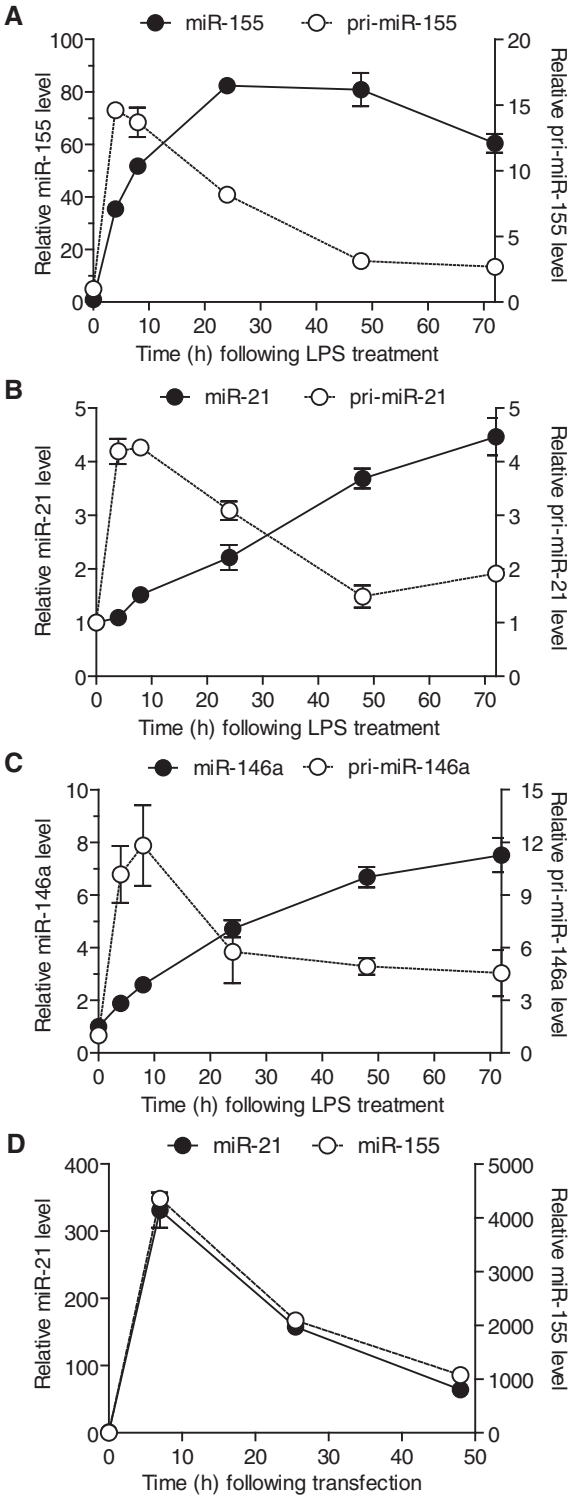

Figure 1. Sustained persistence of innate immune miRNAs in the absence of their precursors. (**A–C**) BMDMs were treated with 10 ng/ml of LPS and incubated for the indicated time before being lysed in RNA extraction buffer. Expression levels of pri- and mature miRNAs were determined by RT-qPCR, reported to that of the internal control (GAPDH and snoRNA-202, for the pri-miRNA and the mature miRNA, respectively) and are shown relative to the values at the initial time-point. The values are averaged from three biological replicates, and are representative of two independent experiments. (**D**) HEK293T-GFP cells were reverse-transfected with 5 nM of both si-miR-21 and si-miR-155 synthetic miRNAs, washed with fresh medium after 7 h and collected in RNA extraction buffer at the indicated times. miRNA levels were determined by RT-qPCR reported to the expression of the house-keeping control RNA miR-16. The values are presented relative to that at the initial time-point, averaged from three biological replicates and are representative of three independent experiments. (**A–D**) Standard error of the mean (SEM) is shown.

Fluorescent-based measure of EGFP knockdown

EGFP down-regulation in MEFs stably expressing EGFP cells was measured using a Fluostar OPTIMA plate-reader as previously reported (23). After 24 h siRNA treatment, the supernatants were discarded and 50 µl of PBS was added to the cells. A standard curve was generated by serially diluting a recombinant EGFP-fusion protein to cover a range from 150 ng/ml to 4.68 ng/ml in 50 µl PBS. EGFP concentration in each well was then inferred from the fluorescence at ex485/em520 correlated to the standard curve, after background autofluorescence (from PBS only) correction.

High-content screening assay

Cell proliferation was assayed using high-content screening assay (HCSA) with a Cellomics ArrayScan HCS Reader (Thermo Fisher Scientific). EGFP cells were counted per captured field according to fluorescent intensity and morphology (with the HCS Reader V-6.6.1.2 software, Thermo Fisher Scientific), up to 3000+ cells per well. The average number of cells per field was used as a quantification of cell number at each time-point.

Mathematical modelling

To build a mathematical model of miRNA degradation independent of recombination efficiency and cell proliferation, we decomposed our analysis in three independent steps. We first established a model of the intracellular miRNA concentration per cell ($y_i = y_1,\ldots,y_n$) following entire blockage of *de novo* miRNA synthesis, function of time ($t_i = t_1,\ldots,t_n$) and assuming that it was solely impacted by the amount of cells that had divided (and that each cell division halved the initial concentration of miRNA). We obtained experimental values from the averaged cell proliferations at different time-points (Supplementary Figure S3B, see 'measured' curve). Relying on this data set, we modelled miRNA decay due to cell proliferation under the assumption that this function is an exponential decay: $F_{\mathrm{cellP}}(t) = \alpha \exp(-ct_i)$, where α is the initial quantity at time t_1, and c is the constant of decay. To identify the co-efficients α and c, we used a non-linear least-square fitting algorithm. The method is based on the minimization of the distance (or error) D between the function $F_{\mathrm{cellP}}(t_i)$ and the data at all points y_i. The distance D is defined as:

$$D(r) = \sum_{i=1}^{n} |F_{\mathrm{cellP}}(t_i,r) - y_i|^2$$

where $r(\alpha, c)$ is the vector with adjustable parameters of function F_{cellP}. The minimization of the function $D(r)$

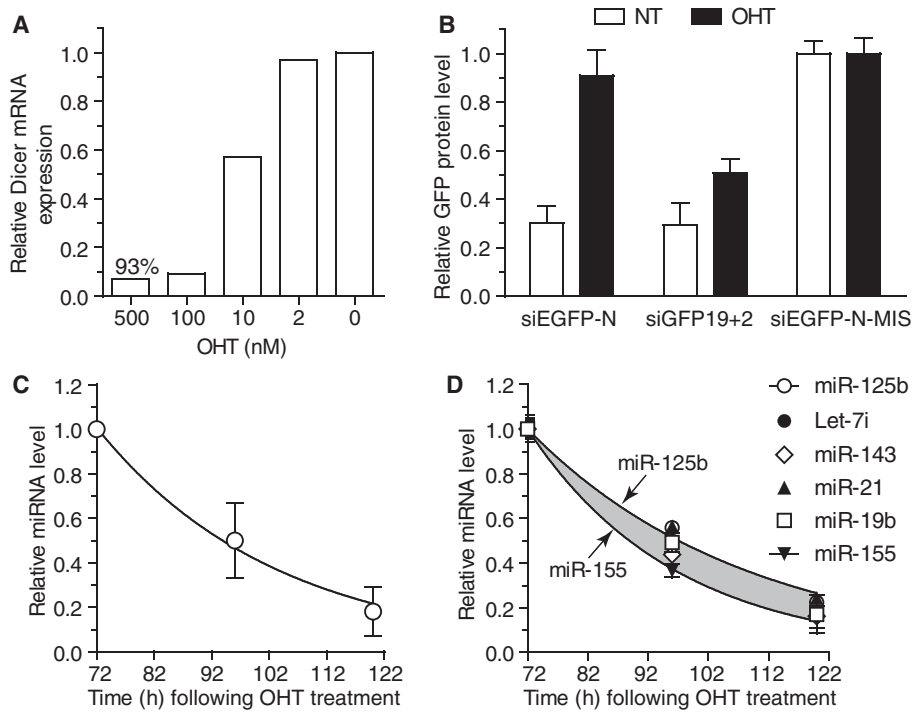

Figure 2. Determination of global miRNA decay. (**A**) Actively dividing *Dicer1*$^{flox/flox}$*xCre/Esr1* MEFs were treated overnight with the indicated concentration of OHT, washed with fresh medium and further incubated for 48 h before being harvested for RNA extraction. Wild-type Dicer1 mRNA was quantified by RT-qPCR and reported to the expression of GAPDH. The data are presented relative to that obtained without OHT treatment (condition '0'), are averaged from biological duplicate and are representative of three independent experiments. (**B**) Actively dividing *Dicer1*$^{flox/flox}$*xCre/Esr1* GFP MEFs were treated (OHT) or not (NT) overnight with 500 nM OHT, and expanded for a further 48 h before being collected and reverse transfected (on Day 3 following initial OHT addition) with 10 nM of the indicated siRNAs. The cells were further incubated for 24 h and EGFP expression was quantified by fluorescent spectrophotometer [see 'Methods' section and (23)]. The data are averaged from two independent experiments in biological triplicate and normalized to the averaged values obtained for the non-targeting siEGFP-N-MIS sequence for each cell type. siEGFP-N-MIS contains two mismatches in the targeting strand of the siRNA compared to siEGFP-N and both siRNAs are Dicer1 substrates (Supplementary Figure S1C); siGFP19+2 is a Dicer1 product (23). (**C** and **D**) Actively dividing *Dicer1*$^{flox/flox}$*xCre/Esr1* MEFs treated with 500 nM OHT were expanded and collected at Days 3–5 following initial OHT treatment. For each miRNA measured, the levels were reported to that obtained at Day 3 ($T = 72$ h following OHT treatment). (**C**) The average level of 104 miRNAs significantly detected by low-density PCR microarray ('Methods' section and Supplementary Table S1) is shown with fitted exponential regression. (**D**) Individual miRNA PCRs were carried out on the samples analysed with low-density PCR microarray and biological replicates. Highlighted in grey is the variation of miRNA decay observed between the six miRNAs analysed, and fitted exponential regression is shown for miR-125 b and miR-155. The data are averaged from biological triplicate and are representative of three independent experiments. SEM (**B** and **D**) and standard deviation (SD) (**C**) are shown.

with respect to the parameter vector r required the zero gradient condition:

$$\nabla D(r) = J^{\mathrm{T}}(F_{\mathrm{cellP}}(r) - y) = 0,$$

where J is Jacobian. The values of the vector r are obtained using the Newton–Raphson iteration method. The process starts with an initial parameter vector r_0 (α_0, c_0) and is corrected to be $r_i = r_0 + \Delta r_i$ in the next iteration. The increment parameter vector Δr therefore satisfies the system of linear equations:

$$\Delta r = -H^{-1} J^{\mathrm{T}}(F_{\mathrm{cellP}}(r) - y)$$

and H can be approximated by $H = J^{\mathrm{T}}J$ for a system with moderate non-linearity.

The second step of modelling defines a function of miRNA intracellular concentration averaged from two distinct cell populations; one population lacking *de novo* miRNA synthesis (ensuing *Dicer1* genetic ablation) $f_1(t) = \beta \exp(-k_1 t)$, and the other that escaped *Dicer1* recombination and producing normal levels of miRNAs $f_2(t) = \beta(1 - k_2 t)$, where β is the initial quantity at the start time t_1. The sum of these two functions models the experimental measurements of the average miRNA concentration per cell y_i at a time t_i. As a result we obtain the function $F(t) = \beta(m \exp(-k_1 t) + (1 - m)(1 - k_2 t))$, where m is the relative proportion of the two cell populations ($0 \leq m \leq 1$), and was experimentally determined by the quantification of wild-type Dicer1 mRNA by RT-PCR (Figure 3A). We estimated parameters k_1, k_2 and β with $m = 0.995$ of recombined cells (Figure 3A and C; 500 nM), applying the non-linear least-square fitting algorithm explained above (the resulting fitted model curve is shown in Figure 3D, FM-99.5%). Next, we validated the relevance of our model by changing the relative proportions of the mixed cell population to $m = 0.5$ (i.e. 50% of recombined cells—Figure 3D, see curve M-50%) and also to $m = 1$ (i.e. where 100% of the cells would lack *de novo* miRNA synthesis and consequently where $F(t) = f_1(t)$, Figure 3D, see curve M-100%).

For the last step of our analysis, we assessed the intracellular miRNA decrease that is independent of that due

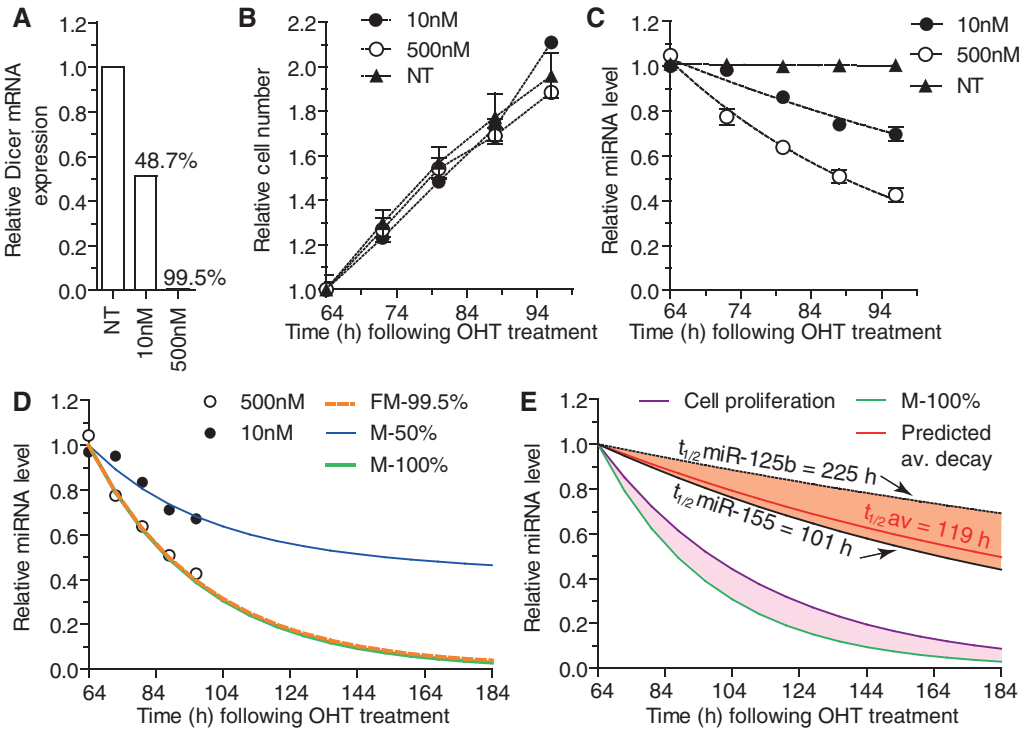

Figure 3. Model of miRNA decay based on experimental measurements. (**A–C**) *Dicer1*$^{flox/flox}$*xCre/Esr1* GFP MEFs were plated at low density (10 000 cells per well of a 6-well plate) and treated for ~16 h with the indicated concentrations of OHT (NT is non-treated). Approximately 64 h following the initial OHT treatment (and every 8 h from then on), some wells were harvested for RNA extraction and cell numbers were quantified using HCSA ('Methods' section). (**A**) GAPDH-normalized wild-type Dicer1 mRNA levels quantified by RT-qPCR were reported to values obtained for NT cells, and used to address the proportion of recombined cells—i.e. Dicer1-deficient cells (indicated in percentage). (**B**) Average cell numbers relative to those at the initial time-point as determined by HCSA are shown from biological triplicate for each cell type with SEM. (**C**) For each individual miRNA, the experimental levels at time T following OHT addition were determined by RT-qPCR normalized to that of snoRNA-202 and relative to the levels obtained in NT cells. The values were further reported to the associated non-linear regression curve at $T = 64$ h (i.e. Day 3) and averages from the six individual miRNAs are shown with SEM. The data are from biological duplicate for each time-point. (**D**) Mathematical fitting to the experimental data set of average miRNA decay obtained with 500 nM OHT (i.e. with 99.5% recombined cells) is shown by the dashed orange line (FM-99.5%) and allowed for the determination of modelled miRNA decay in 50% and 100% recombined cell populations (M-50% and M-100% curves). Noteworthy, M-50% closely matched the experimental average miRNA decay with 48.7% recombined cells obtained with the 10 nM OHT condition. (**E**) Following the determination of M-100% and miRNA decay relating to cell proliferation (Cell proliferation—see Modelling in 'Methods' section), we determined the 'absolute' miRNA decay in a theoretical non-dividing cell (highlighted in purple) for the average of the six miRNAs (Predicted av. decay) and inferred the average half-life of miRNA ($t_{1/2}$ av = 119 h). The predicted decays of miR-125b and miR-155 are also shown; highlighted in orange is the variation of miRNA decay observed between the six miRNAs analysed. The experimental data used for the modelling are representative of two independent experiments.

to cell division—referred to as the 'absolute' miRNA decay. We established a function of the difference between the function of miRNA decrease solely due to cell proliferation $F_{\text{cellP}}(t)$ and the function of miRNA decrease inferred from our experiments in a cell population entirely lacking *de novo* miRNA synthesis $F(t) = f_1(t)$ where $m = 1$. We assumed from our observations in BMDMs that such 'absolute' miRNA degradation function fits an exponential decay (Figure 4C), and specified the following:

$$F_{\text{absolute}}(t) = \gamma \exp(-\mathrm{d}t).$$

To determine the co-efficients γ and d, we relied on the fact that experimentally inferred $F(t)$ is included in the $F_{\text{absolute}}(t)$ and the miRNA decrease due to cell proliferation $F_{\text{cellP}}(t)$. Hence

$$F(t) = F_{\text{cellP}}(t) - F_{\text{absolute}}(t), \text{ or } F(t) = z\exp(-\mathrm{c}t_i) - \gamma\exp(-\mathrm{d}t).$$

We determined the parameters z, γ and d relying on the same non-linear fitting algorithm. The 'absolute' miRNA half-life, independent of cell proliferation in a cell population entirely devoid of *de novo* miRNA synthesis, was then calculated based on the decay constant d as follows:

$$t_{1/2} = \frac{\ln(2)}{\mathrm{d}}.$$

RESULTS

Persistence of miR-155, miR-146 a and miR-21

With the aim of better understanding their role in the regulation of macrophage function, we originally investigated the persistence of three miRNAs (miR-155, miR-146 a and miR-21) that are rapidly induced in immune cells following stimulation with pathogen-derived products (26,27). Stimulation of primary BMDMs with

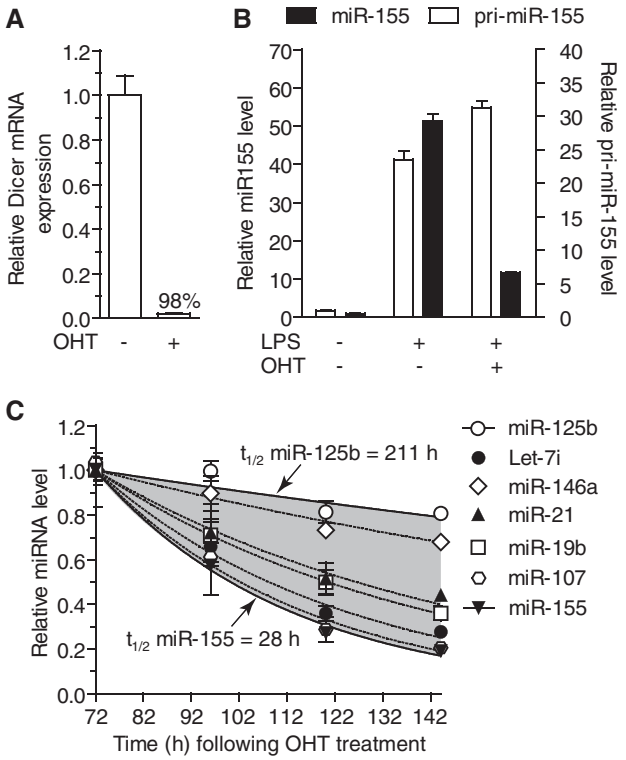

Figure 4. Widespread variation of miRNA decay in slow dividing primary macrophages. (**A–C**) BMDMs from *Dicer1*$^{flox/flox}$*xCre/Esr1* mice were treated (OHT +) or not (OHT −) for 48 h with 500 nM OHT as described in 'Methods' section. The cells were collected every 24 h from Day 3 ($T = 72$ h) following initial OHT addition. (**A**) GAPDH-normalized wild-type Dicer1 mRNA levels quantified by RT-qPCR were reported to values obtained for NT cells on Day 3 in biological triplicate. (**B**) OHT-treated (+) or not (−) BMDMs were stimulated with 10 ng/ml LPS (+) or not (LPS −) for 6 h and collected for RNA extraction. GAPDH-normalized pri-miR-155 and snoRNA-202 normalized miR-155 levels are shown relative to the values obtained in non-OHT and non-LPS stimulated cells from biological triplicate. (**C**) Seven miRNAs were measured from biological triplicate of cells stimulated with OHT, normalized to snoRNA-202 and reported to the initial values at $T = 72$ h (i.e. Day 3 following initial OHT treatment). Highlighted in grey is the variation of miRNA decay observed between the seven miRNAs analysed, and fitted exponential regression with halving-time is shown for miR-125b and miR-155. (**A–C**) SEM is shown.

lipopolysaccharide (LPS) resulted in the rapid and transient induction of the respective primary transcripts of each miRNA (with a peak of expression between 4 h and 8 h returning to lower levels by 24 h) (Figures 1A–C). Conversely, the overall levels of the three mature miRNAs accumulated over the 48–72 h period, with the exception of miR-155 which decreased by 25% after 48 h (that is ~40 h after the initial decrease of pri-miR-155). This discrepancy between precursor and mature miRNA levels indicated that degradation of mature miRNAs was much slower than the upstream processing of pri-miRNAs. Similar observations were made for miR-155 and miR-21 in splenic B cells, supporting the concept that the persistence of these miRNAs was not cell specific (Supplementary Figure S1A and B). To rule out a putative specific stabilization of the induced forms of these miRNAs, we next addressed the stability of transfected synthetic mature miRNA mimics (si-miRNAs). Such mimics are based on a duplex with 3′-2 nt overhang consisting of the mature miRNA sequence and its perfectly matching complementary strand and have been shown to recapitulate localization and degradation similar to that of mature miRNAs (28). Following transfection of the si-miRNAs into HEK293 cells, we observed that the decrease of mature miR-155 and miR-21 levels (which exceeded their respective basal endogenous levels by several 100-fold—Figure 1D compare 0 and 7 h time-points) was also relatively slow (~50% in 17 h) and in fact could mostly be attributed to cell division (Figure 1D, and data not shown). Collectively, these results suggested that the mature forms of miR-155, miR-21 and miR-146 a were long-lived following processing, independently of their expression.

Global persistence of miRNA following Dicer1 processing

The impressive stability of miR-155, miR-21 and miR-146 a in BMDMs prompted us to investigate the global persistence of mature miRNAs, and to address whether this persistence is the rule or an exception. To establish a cell model where miRNA stability could be measured following ablation of miRNA final processing step, we exploited *Dicer1* genetic deletion. Accordingly, *Dicer1*$^{flox/flox}$*xCre/Esr1* mice, in which the majority of the second RNase III domain of Dicer1 can ubiquitously be deleted following OHT treatment, thus resulting in ablation of Dicer1 activity (21,22) were used. In a similar mouse model to the one described here, *Dicer1* ablation by OHT treatment of mouse MEFs has previously been shown to promote p53 induction and decrease cell proliferation, thus compromising survival of these cells (29). Since MEF immortalization through expression of the simian virus 40 large T-antigen (SV40 TAg) results in p53 inactivation (30) and yields rapidly dividing stable cell lines, we posited that TAg immortalization of MEFs from *Dicer1*$^{flox/flox}$*xCre/Esr1* mice would mostly rescue cell survival on OHT treatment.

Following TAg immortalization of *Dicer1*$^{flox/flox}$*xCre/Esr1* MEFs, the ability of OHT to induce *Dicer1* genomic ablation was tested. Importantly, 500 nM OHT treatment of the cells resulted in the robust recombination of the cells (at least >93% in all experiments) as measured through the levels of remaining wild-type Dicer1 mRNA (Figure 2A). In accord with TAg-inhibition of p53-induced cell death following Dicer1 ablation, cell proliferation was unaffected within 90–120 h following OHT treatment (data not shown). However, the MEFs stopped proliferating after 170–190 h of culture in medium supplemented with 100 nM OHT (i.e. 6–8 cell divisions), confirming previous observations (29). To confirm loss of processing of pre-miRNAs, the ability of a Dicer1-substrate small interfering RNA (D-siEGFP) to promote RNA interference against EGFP stably expressed by the cells was measured. Such a Dicer1-substrate is based on a 25-nt sense strand complementary to a 27-nt targeting strand, generating an asymmetric duplex with one overhang and one blunt end (Supplementary Figure S1B). This design allows for specific Dicer1 cleavage and enhanced selection of the

targeting strand (31). Importantly, RNAi efficiency directly relates to Dicer1 processing of these asymmetric siRNAs (31). In our experiments, D-siEGFP lost its ability to trigger EGFP down-regulation 3 days post-OHT treatment, suggesting ablation of Dicer1 activity and *de novo* miRNA synthesis was ineffective from then on (Figure 2B).

To capture a global trend of the variations of miRNA levels following ablation of Dicer1 processing, RNA was collected from actively dividing cells at Days 3–5 post-OHT treatment and the expression of 335 mouse miRNAs was analysed with TaqMan® RT-qPCR low density arrays. In this preliminary screen, we identified 104 miRNAs expressed at significant levels in the cells, which were consistently decreased with time ('Methods' and Supplementary Table S1). The average decrease of intracellular miRNA concentration for these 104 miRNAs was constant between Days 3 and 4, and 4 and 5, and followed an exponential decrease curve with a halving-time of 21.6 h (Figure 2C). The robustness of the RT-qPCR arrays was validated by individually measuring the levels of a panel of six miRNAs (with varying basal abundance) (Figure 2D; Supplementary Figure S2A). A good correlation (0.88) was seen between individual PCRs and PCR-arrays and the average decrease halving-time for these six miRNAs was also 21.6 h, indicating that this panel of miRNAs gave a good representation of the global trend of miRNA decrease (Figure 2D and Supplementary Figure S2B). Noteworthy, the exponential trend of miRNA decrease was closely correlated with miRNA intracellular concentration being related to cellular division.

Modelling of miRNA decay

Having identified a panel of miRNAs representing the global trend of miRNA decay, we set out to establish a model of miRNA degradation compensating for the loss of miRNA per cell due to cell division. In addition, the impact of the residual cell population that evades OHT treatment and produces normal levels of miRNAs was also taken into account. Samples were collected from MEFs treated with two different doses of OHT, and the levels of the six miRNAs measured with time, and cell proliferation assessed (Figure 3A–C and Supplementary Figure S3). Using exponential fitting to the averaged experimental data from the six miRNAs (Figure 3C), we first established a model of miRNA decrease in the samples treated with 500 nM OHT in which 99.5% of the cells lost Dicer1 expression (Figure 3A and D, see FM-99.5% curve and 'Methods' section). To confirm the validity of the mathematical prediction of miRNA decay function of cell recombination, we modelled miRNA decrease in a situation where 50% of the cells had recombined (M-50%—Figure 3D). The resulting predicted miRNA decrease closely matched the experimental data set where 48.7% of the cells had recombined, obtained with 10 nM OHT (Figure 3D—compare M-50% curve and the distribution of 10 nM experimental points). This suggested faithful modelling of miRNA intracellular decrease function of cell recombination, and allowed us to infer miRNA decrease in a hypothetic pure cell population (with 100%-*Dicer1*-deficient cells—Figure 3D, see M-100%).

The analysis of cell proliferation confirmed that OHT treatment did not significantly impact on cell growth over the course of the experiment (Figure 3B—compare 500 nM OHT-treated and non-treated cells). Relying on this experimental determination of cell proliferation, a model of miRNA decrease as a function of cell division was established, assuming that each divided cell received half the initial intracellular content of miRNAs (Supplementary Figure S3B and 'Methods' section). Subtraction of this function from the predicted miRNA decrease in pure cell population (M-100%) resulted in the model of miRNA decay, independent of cell proliferation, as a function of time (Figure 3E, see 'predicted av. decay' curve). Based on the averaged experimental measurements of the panel of six miRNAs, the theoretic average miRNA half-life thus obtained was 119 h (~5 days). Importantly, we noticed large differences in predicted half-lives, ranging from ~101 h for miR-155 (~4 days), up to 225 h (~9 days) for miR-125b, suggesting that although generally extremely stable, some miRNA sequences were significantly more stable than others following Dicer1 processing (Figure 3E—compare miR-125b and miR-155, and Supplementary Figure S3C).

miRNA persistence varies between miRNAs

To investigate further the observations that some miRNAs are more persistent than others in non-dividing cells and to validate the relevance of the predicted miRNA half-life, the decay rates of miRNA following *Dicer1* ablation were measured in slow dividing primary BMDMs. OHT treatment of BMDMs from *Dicer1*$^{flox/flox}$*xCre/Esr1* mice promoted *Dicer1* genomic ablation in >98% of the cells as seen with the levels of wild-type Dicer1 mRNA 3 days after OHT treatment (Figure 4A). To determine the point in time at which Dicer1 enzymatic processing of pre-miRNA was ablated following OHT-induced *Dicer1* genetic deletion, LPS treatment of BMDMs was used to induce the miR-155 pri and mature forms (Figure 4B). Processing of pri-miR-155 into mature miR-155 was strongly impeded 3 days after OHT treatment when compared to the non-OHT-treated cells, although a small proportion of *de novo* miR-155 could still be synthesized indicating that some cells still exerted Dicer1 enzymatic activity at this point in time. Quantification of the average basal levels of seven miRNAs with varying abundance from Day 3 following OHT treatment confirmed the great stability of miRNAs following Dicer1 processing (Figure 4C). However, in agreement with our predictions from the measurement of miRNA levels in MEFs, we observed that miRNAs decayed with varying kinetics (the fastest and slowest being miR-155/miR-107 and miR-125b, respectively) (Figure 4C). Collectively, these results support the notion that although generally extremely stable, miRNAs are turned over with varying rates following synthesis.

DISCUSSION

The steady-state level of miRNA is influenced by three main parameters: transcription, processing and decay. The last decade has seen a remarkable effort to characterize the parameters that affect the transcriptional activity of select miRNAs, and more recently, their processing, highlighting sophisticated mechanisms of control (8). It is proposed that a minimum of 100 molecules of miRNAs per cell are required for their translational regulatory effects (10,32). Control of steady-state miRNA concentration therefore directly relates to the control of miRNA function. Interestingly, although crucial for the regulation of steady-state miRNA levels, little has been uncovered about the regulation of miRNA half-life and stability in the cell, following processing. In analogy to what is seen with mRNA (33), it can be speculated that determining the half-life of a given miRNA could directly inform on its biological function.

Stimulation of immune cells with pathogen-derived products results in the nuclear factor κ-B-dependent rapid induction of mature miR-155, miR-146a and miR-21 (26,34). The strict regulation of nuclear factor κ-B transcriptional activity results in the transient induction of most of its targets, and we show here that the primary transcripts of these three miRNAs are consistent with this (Figures 1A–C). However, the mature form of these miRNAs accumulated in the cells and persisted at high levels in the absence of induced precursors. It is worth noting here that miR-155 appeared to be less stable than miR-21 and miR-146a and was the only miRNA to decrease over the 72 h of observation (Figure 1A). This stability was not exclusive of the induced forms of these miRNAs, as transfection of synthetic miRNAs confirmed that the mature forms of miR-155 and miR-21 were detectable >48 h after transfection (Figure 1D). Similar observations were made in primary B cells, indicating that the persistence of these miRNAs following induction was not restricted to BMDMs (Supplementary Figure S1).

To determine whether the persistence of these three miRNAs was the rule or an exception, we investigated the global decay of miRNAs following synthesis. Although other studies have used traditional transcriptional shutdown experiments to determine miRNA decay rates in different cell lines (NIH3T3, RPE-1, ES cells and HEK293 cells), these attempts failed to measure any significant decrease of miRNA concentrations over the course of their experimental set-up (14,35). We reasoned that the extent of miRNA half-life was such that transcriptional shutdown-type experiments could not be prolonged enough to allow for an accurate determination of miRNA decay. An alternative approach to global transcriptional shutdown is the selective blocking of miRNA maturation by Dicer1, through ablation of Dicer1 enzymatic activity. Our analysis of 104 miRNAs by TaqMan® RT-qPCR, the current gold standard for miRNA quantification (36), indicated that the global miRNA decrease followed an exponential function with a half-life of 21.6 h, following loss of Dicer1 enzymatic activity. These findings strongly supported the concept that intracellular miRNA levels were mostly affected by dilution from cellular division. Noteworthy, we found 27 miRNAs that were only detected on Day 3, possibly reflecting their more rapid decay as previously proposed for miR-382 (35) (Supplementary Table S1, 'Rapily degraded?'). Further analyses would be required to draw specific conclusions on the behaviour of individual miRNAs identified in this preliminary screen.

In order to calculate miRNA half-life independent of cellular division and any residual Dicer1 activity, the decay rates of a representative panel of six miRNAs were measured in two populations of cells with varying *Dicer1* recombination efficiency (one population averaging 50%, the other 99.5%) and a mathematical model established to predict miRNA stability in a hypothetical non-dividing cell population entirely devoid of Dicer1 function (Figure 3). Correction of cell proliferation revealed an extreme stability of miRNAs with a modelled half-life of 119 h (~5 days) for the averaged panel of miRNAs—ranging with individual modelling from ~ 99 h and 101 h for let-7i and miR-155, up to 225 h (~9 days) for miR-125b (see Supplementary Figure S3C for modelled persistence of individual miRNAs studied). These predictions of miRNA stability in non-dividing cells are in line with other reports demonstrating that *in vivo* half-life of mature miR-208 could extend up to 12 days (12), or that the half-life of miRNA-loaded RISC complexes could average ~140 h (~6 days) following inducible shutdown of an artificial miRNA expression (37). To confirm further the relevance of modelling of miRNA persistence, miRNA decay was investigated in slow-dividing primary BMDMs following *Dicer1* ablation (Figure 4C). Due to the limited division of these cells, we were able to establish a more relevant picture of miRNA decay kinetics for specific miRNAs without the need for mathematical correction. Consistent with the studies performed in MEFs (Figures 2D and 3E), miR-155 and miR-125b exerted very different stabilities in BMDMs. While the half-life of miR-125b was 211 h, i.e. ~9 days (which is concordant with our modelled half-life for this miRNA), that of miR-155 was only ~28 h, i.e. 3.5× less that predicted from the MEFs model for this miRNA. This suggests that miRNA stability might be differentially regulated in different cell types—with BMDMs having a more rapid turnover of a subset of select miRNAs. In agreement with our initial observations of miRNA stability following induction (Figure 1), basal levels of miR-21 and miR-146a were significantly more stable than that of miR-155 following *Dicer1* ablation in BMDMs (Figure 4C). Although all three miRNAs are rapidly induced to similar intracellular levels following innate immune activation [(38) and data not shown], these results indicate that miR-155 is intrinsically less stable than miR-21 and miR-146a, and consequently has less sustained regulatory effects.

Collectively, our data demonstrate that although >10× more stable than mRNA (the median half-life of which is ~10 h (33), some miRNAs such as miR-125b are more persistent than others. Increased stability of select miRNAs is unlikely to be related to a 3′ modification of these miRNAs, as indicated by a recent genome-wide study that failed to demonstrate an impact of 3′

adenylation on miRNA stability (39). Preferential active degradation of select miRNAs could be at play, however the miRNA decay machinery characterized to date was not found to be able to differentiate between miRNAs (11,17). In their elegant work, Krol *et al*. (14) recently demonstrated the rapid intracellular decrease of all miRNAs measured following transcriptional shutdown, in different types of neurons (e.g. from retina and cortex). Intriguingly, the rapid decrease (within a couple of hours) of intracellular miRNAs was only partial and 40–50% of initial levels remained untouched (8,14). Thus a portion of miRNAs present in neurons could be subject to rapid turnover while the rest would not, for instance because of their subcellular localization (8). Accordingly, we speculate that the decrease of the remaining 40–50% of each miRNA (which are not affected by transcriptional shutdown) in neurons would have much slower kinetics, possibly similar to what we observe in our model of non-dividing cells (i.e. ~5–9 days). In fact, persistence of select miRNAs for up to 2 months following *Dicer1* ablation has been reported in neurons *in vivo* (40). Several reports have suggested the rapid intracellular (within 4–8 h) decrease of select miRNAs following stimulation, such as innate immune recruitment (41–46). For instance, levels of miR-125b were commonly found to rapidly decrease (within 4–6 h) in murine phagocytes stimulated by LPS, by miRNA microarray and miRNA RT-qPCR analyses (41,44). However, we failed to measure such a rapid decrease in BMDMs stimulated with LPS, although the differences could originate from differences between the cells used and their *in vitro* differentiation (data not shown). Assuming such a rapid decay of miR-125b, our findings regarding the persistence of miR-125b indicate the selective active decay of this miRNA following stimulation. Whether or not machinery with preferential active degradation of select miRNAs could carry out this task remains to be determined, but this has been proposed to be the case for miR-382 (35).

In summary, this work establishes the average miRNA half-life independent of cell proliferation and provides direct evidence that miRNA turnover can vary widely among miRNAs. Recent insight into the regulation of miRNA-mediated control of mRNA translation in mammalian cells has revealed that miRISC binding to target mRNAs predominantly results in decreased mRNA levels (47), and thereby mostly impacts on mRNA stability. Whether or not the stability of a given miRNA correlates with the overall half-life of its targets would be worthwhile investigating, and might be informative on the biological significance of the variable persistence between miRNAs reported here. For instance, the finding that miR-155 is less stable than miR-146a and miR-21 highlights further the different biological functions of these innate immune miRNAs. Given that miRNA persistence is a function of the miRNA and also the cell type considered, our work stresses the need for the detailed characterization of a target miRNA turnover, for translational approaches aiming at blocking miRNA function through the use of synthetic antagomirs. Our observations strongly suggest that miRNA persistence relates to biological function, and that better characterization of miRNA stability and associated regulatory mechanisms should provide new avenues for the characterization of their biological functions.

SUPPLEMENTARY DATA

Supplementary Data are available at NAR Online.

ACKNOWLEDGEMENTS

We are grateful to D.N. Watkins (Monash Institute of Medical Research) for the gift of the *R26CreER* mice, and to K. Herron (Applied Biosystems, Mulgrave, Australia) and T. Wilson (Monash Institute of Medical Research) for their help with TaqMan® PCR low density arrays and high-content screening assays, respectively.

FUNDING

The Australian National Health and Medical Research Council (491106, 606425 and 1006590 to B.R.G.W.); Victorian Government's Operational Infrastructure Support Program; Health Research Board Ireland (to C.E.M.). Funding for open access charge: Monash Institute of Medical Research.

Conflict of interest statement. M.A.B is employed by Integrated DNA Technologies Inc. (IDT), which offers oligonucleotides for sale similar to some of the compounds described in the manuscript. IDT is, however, not a publicly traded company, and he does not own any shares or hold equity in IDT.

REFERENCES

1. Umbach,J.L. and Cullen,B.R. (2009) The role of RNAi and microRNAs in animal virus replication and antiviral immunity. *Genes Dev*., **23**, 1151–1164.
2. Bernstein,E., Kim,S.Y., Carmell,M.A., Murchison,E.P., Alcorn,H., Li,M.Z., Mills,A.A., Elledge,S.J., Anderson,K.V. and Hannon,G.J. (2003) Dicer is essential for mouse development. *Nat. Genet*., **35**, 215–217.
3. Yang,W.J., Yang,D.D., Na,S., Sandusky,G.E., Zhang,Q. and Zhao,G. (2005) Dicer is required for embryonic angiogenesis during mouse development. *J. Biol. Chem*., **280**, 9330–9335.
4. Croce,C.M. (2009) Causes and consequences of microRNA dysregulation in cancer. *Nat. Rev. Genet*., **10**, 704–714.
5. Lee,Y., Ahn,C., Han,J., Choi,H., Kim,J., Yim,J., Lee,J., Provost,P., Radmark,O., Kim,S. *et al*. (2003) The nuclear RNase III Drosha initiates microRNA processing. *Nature*, **425**, 415–419.
6. Bernstein,E., Caudy,A.A., Hammond,S.M. and Hannon,G.J. (2001) Role for a bidentate ribonuclease in the initiation step of RNA interference. *Nature*, **409**, 363–366.
7. Filipowicz,W., Bhattacharyya,S.N. and Sonenberg,N. (2008) Mechanisms of post-transcriptional regulation by microRNAs: are the answers in sight? *Nat. Rev. Genet*., **9**, 102–114.
8. Krol,J., Loedige,I. and Filipowicz,W. (2010) The widespread regulation of microRNA biogenesis, function and decay. *Nat. Rev. Genet*., **11**, 597–610.
9. Heo,I., Joo,C., Cho,J., Ha,M., Han,J. and Kim,V.N. (2008) Lin28 mediates the terminal uridylation of let-7 precursor MicroRNA. *Mol. Cell*, **32**, 276–284.

10. Brown,B.D., Gentner,B., Cantore,A., Colleoni,S., Amendola,M., Zingale,A., Baccarini,A., Lazzari,G., Galli,C. and Naldini,L. (2007) Endogenous microRNA can be broadly exploited to regulate transgene expression according to tissue, lineage and differentiation state. *Nat. Biotechnol.*, **25**, 1457–1467.
11. Kai,Z.S. and Pasquinelli,A.E. (2010) MicroRNA assassins: factors that regulate the disappearance of miRNAs. *Nat. Struct. Mol. Biol.*, **17**, 5–10.
12. van Rooij,E., Sutherland,L.B., Qi,X., Richardson,J.A., Hill,J. and Olson,E.N. (2007) Control of stress-dependent cardiac growth and gene expression by a microRNA. *Science*, **316**, 575–579.
13. Gatfield,D., Le Martelot,G., Vejnar,C.E., Gerlach,D., Schaad,O., Fleury-Olela,F., Ruskeepaa,A.L., Oresic,M., Esau,C.C., Zdobnov,E.M. *et al.* (2009) Integration of microRNA miR-122 in hepatic circadian gene expression. *Genes Dev.*, **23**, 1313–1326.
14. Krol,J., Busskamp,V., Markiewicz,I., Stadler,M.B., Ribi,S., Richter,J., Duebel,J., Bicker,S., Fehling,H.J., Schubeler,D. *et al.* (2010) Characterizing light-regulated retinal microRNAs reveals rapid turnover as a common property of neuronal microRNAs. *Cell*, **141**, 618–631.
15. Katoh,T., Sakaguchi,Y., Miyauchi,K., Suzuki,T., Kashiwabara,S., Baba,T. and Suzuki,T. (2009) Selective stabilization of mammalian microRNAs by 3′ adenylation mediated by the cytoplasmic poly(A) polymerase GLD-2. *Genes Dev.*, **23**, 433–438.
16. Ameres,S.L., Horwich,M.D., Hung,J.H., Xu,J., Ghildiyal,M., Weng,Z. and Zamore,P.D. (2010) Target RNA-directed trimming and tailing of small silencing RNAs. *Science*, **328**, 1534–1539.
17. Chatterjee,S. and Grosshans,H. (2009) Active turnover modulates mature microRNA activity in Caenorhabditis elegans. *Nature*, **461**, 546–549.
18. Cheloufi,S., Dos Santos,C.O., Chong,M.M. and Hannon,G.J. (2010) A dicer-independent miRNA biogenesis pathway that requires Ago catalysis. *Nature*, **465**, 584–589.
19. Hutvagner,G., McLachlan,J., Pasquinelli,A.E., Balint,E., Tuschl,T. and Zamore,P.D. (2001) A cellular function for the RNA-interference enzyme Dicer in the maturation of the let-7 small temporal RNA. *Science*, **293**, 834–838.
20. Yi,R., Pasolli,H.A., Landthaler,M., Hafner,M., Ojo,T., Sheridan,R., Sander,C., O'Carroll,D., Stoffel,M., Tuschl,T. *et al.* (2009) DGCR8-dependent microRNA biogenesis is essential for skin development. *Proc. Natl Acad. Sci. USA*, **106**, 498–502.
21. Harfe,B.D., McManus,M.T., Mansfield,J.H., Hornstein,E. and Tabin,C.J. (2005) The RNaseIII enzyme Dicer is required for morphogenesis but not patterning of the vertebrate limb. *Proc. Natl Acad. Sci. USA*, **102**, 10898–10903.
22. Badea,T.C., Wang,Y. and Nathans,J. (2003) A non-invasive genetic/pharmacologic strategy for visualizing cell morphology and clonal relationships in the mouse. *J. Neurosci.*, **23**, 2314–2322.
23. Gantier,M.P., Tong,S., Behlke,M.A., Irving,A.T., Lappas,M., Nilsson,U.W., Latz,E., McMillan,N.A. and Williams,B.R. (2010) Rational design of immunostimulatory siRNAs. *Mol. Ther.*, **18**, 785–795.
24. O'Connell,R.M., Chaudhuri,A.A., Rao,D.S. and Baltimore,D. (2009) Inositol phosphatase SHIP1 is a primary target of miR-155. *Proc. Natl Acad. Sci. USA*, **106**, 7113–7118.
25. Chiang,H.R., Schoenfeld,L.W., Ruby,J.G., Auyeung,V.C., Spies,N., Baek,D., Johnston,W.K., Russ,C., Luo,S., Babiarz,J.E. *et al.* (2010) Mammalian microRNAs: experimental evaluation of novel and previously annotated genes. *Genes Dev.*, **24**, 992–1009.
26. Sheedy,F.J., Palsson-McDermott,E., Hennessy,E.J., Martin,C., O'Leary,J.J., Ruan,Q., Johnson,D.S., Chen,Y. and O'Neill,L.A. (2010) Negative regulation of TLR4 via targeting of the proinflammatory tumor suppressor PDCD4 by the microRNA miR-21. *Nat. Immunol.*, **11**, 141–147.
27. McCoy,C.E., Sheedy,F.J., Qualls,J.E., Doyle,S.L., Quinn,S.R., Murray,P.J. and O'Neill,L.A. (2010) IL-10 inhibits miR-155 induction by toll-like receptors. *J. Biol. Chem.*, **285**, 20492–20498.
28. Hwang,H.W., Wentzel,E.A. and Mendell,J.T. (2007) A hexanucleotide element directs microRNA nuclear import. *Science*, **315**, 97–100.
29. Mudhasani,R., Zhu,Z., Hutvagner,G., Eischen,C.M., Lyle,S., Hall,L.L., Lawrence,J.B., Imbalzano,A.N. and Jones,S.N. (2008) Loss of miRNA biogenesis induces p19Arf-p53 signaling and senescence in primary cells. *J. Cell. Biol.*, **181**, 1055–1063.
30. Sachsenmeier,K.F. and Pipas,J.M. (2001) Inhibition of Rb and p53 is insufficient for SV40 T-antigen transformation. *Virology*, **283**, 40–48.
31. Rose,S.D., Kim,D.H., Amarzguioui,M., Heidel,J.D., Collingwood,M.A., Davis,M.E., Rossi,J.J. and Behlke,M.A. (2005) Functional polarity is introduced by Dicer processing of short substrate RNAs. *Nucleic Acids Res.*, **33**, 4140–4156.
32. Sarasin-Filipowicz,M., Krol,J., Markiewicz,I., Heim,M.H. and Filipowicz,W. (2009) Decreased levels of microRNA miR-122 in individuals with hepatitis C responding poorly to interferon therapy. *Nat. Med.*, **15**, 31–33.
33. Yang,E., van Nimwegen,E., Zavolan,M., Rajewsky,N., Schroeder,M., Magnasco,M. and Darnell,J.E. Jr (2003) Decay rates of human mRNAs: correlation with functional characteristics and sequence attributes. *Genome Res.*, **13**, 1863–1872.
34. O'Connell,R.M., Rao,D.S., Chaudhuri,A.A. and Baltimore,D. (2010) Physiological and pathological roles for microRNAs in the immune system. *Nat. Rev. Immunol.*, **10**, 111–122.
35. Bail,S., Swerdel,M., Liu,H., Jiao,X., Goff,L.A., Hart,R.P. and Kiledjian,M. (2010) Differential regulation of microRNA stability. *RNA*, **16**, 1032–1039.
36. Meyer,S.U., Pfaffl,M.W. and Ulbrich,S.E. (2010) Normalization strategies for microRNA profiling experiments: a 'normal' way to a hidden layer of complexity? *Biotechnol. Lett.*, **32**, 1777–1788.
37. Berger,S.M., Pesold,B., Reber,S., Schonig,K., Berger,A.J., Weidenfeld,I., Miao,J., Berger,M.R., Gruss,O.J. and Bartsch,D. (2010) Quantitative analysis of conditional gene inactivation using rationally designed, tetracycline-controlled miRNAs. *Nucleic Acids Res.*, **38**, e168.
38. Gantier,M.P. (2010) New perspectives in MicroRNA regulation of innate immunity. *J Interferon Cytokine Res.*, **30**, 283–289.
39. Burroughs,A.M., Ando,Y., de Hoon,M.J., Tomaru,Y., Nishibu,T., Ukekawa,R., Funakoshi,T., Kurokawa,T., Suzuki,H., Hayashizaki,Y. *et al.* (2010) A comprehensive survey of 3′ animal miRNA modification events and a possible role for 3′ adenylation in modulating miRNA targeting effectiveness. *Genome Res.*, **20**, 1398–1410.
40. Schaefer,A., O'Carroll,D., Tan,C.L., Hillman,D., Sugimori,M., Llinas,R. and Greengard,P. (2007) Cerebellar neurodegeneration in the absence of microRNAs. *J. Exp. Med.*, **204**, 1553–1558.
41. Ceppi,M., Pereira,P.M., Dunand-Sauthier,I., Barras,E., Reith,W., Santos,M.A. and Pierre,P. (2009) MicroRNA-155 modulates the interleukin-1 signaling pathway in activated human monocyte-derived dendritic cells. *Proc. Natl Acad. Sci. USA*, **106**, 2735–2740.
42. Zhou,R., Hu,G., Liu,J., Gong,A.Y., Drescher,K.M. and Chen,X.M. (2009) NF-kappaB p65-dependent transactivation of miRNA genes following *Cryptosporidium parvum* infection stimulates epithelial cell immune responses. *PLoS Pathog.*, **5**, e1000681.
43. Ruggiero,T., Trabucchi,M., De Santa,F., Zupo,S., Harfe,B.D., McManus,M.T., Rosenfeld,M.G., Briata,P. and Gherzi,R. (2009) LPS induces KH-type splicing regulatory protein-dependent processing of microRNA-155 precursors in macrophages. *FASEB J.*, **23**, 2898–2908.
44. Androulidaki,A., Iliopoulos,D., Arranz,A., Doxaki,C., Schworer,S., Zacharioudaki,V., Margioris,A.N., Tsichlis,P.N. and Tsatsanis,C. (2009) The kinase Akt1 controls macrophage response to lipopolysaccharide by regulating microRNAs. *Immunity*, **31**, 220–231.
45. Chen,X.M., Splinter,P.L., O'Hara,S.P. and LaRusso,N.F. (2007) A cellular micro-RNA, let-7i, regulates Toll-like receptor 4 expression and contributes to cholangiocyte immune responses against Cryptosporidium parvum infection. *J. Biol. Chem.*, **282**, 28929–28938.

46. Tili,E., Michaille,J.J., Cimino,A., Costinean,S., Dumitru,C.D., Adair,B., Fabbri,M., Alder,H., Liu,C.G., Calin,G.A. *et al*. (2007) Modulation of miR-155 and miR-125b levels following lipopolysaccharide/TNF-alpha stimulation and their possible roles in regulating the response to endotoxin shock. *J. Immunol.*, **179**, 5082–5089.

47. Guo,H., Ingolia,N.T., Weissman,J.S. and Bartel,D.P. (2010) Mammalian microRNAs predominantly act to decrease target mRNA levels. *Nature*, **466**, 835–840.

Author/s:
Gantier, MP;McCoy, CE;Rusinova, I;Saulep, D;Wang, D;Xu, D;Irving, AT;Behlke, MA;Hertzog, PJ;Mackay, F;Williams, BRG

Title:
Analysis of microRNA turnover in mammalian cells following Dicer1 ablation

Date:
2011-07-01

Citation:
Gantier, M. P., McCoy, C. E., Rusinova, I., Saulep, D., Wang, D., Xu, D., Irving, A. T., Behlke, M. A., Hertzog, P. J., Mackay, F. & Williams, B. R. G. (2011). Analysis of microRNA turnover in mammalian cells following Dicer1 ablation. NUCLEIC ACIDS RESEARCH, 39 (13), pp.5692-5703. https://doi.org/10.1093/nar/gkr148.

Persistent Link:
http://hdl.handle.net/11343/261899